UNIVERSIDAD NACIONAL DE COLOMBIA
SEDE MEDELLÍN
FACULTAD DE MINAS

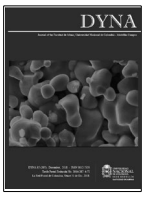

DYNA
http://dyna.medellin.unal.edu.co/

Constitutive simulation of a Kaolin clay with vertical and horizontal sedimentation axes

William Mario Fuentes-Lacouture, José Alejandro Duque-Felfle & Carlos José Lascarro-Estrada

Departamento de Ingeniería Civil y Ambiental, Universidad del Norte, Barranquilla, Colombia. fuentesw@uninorte.edu.co, jfelfle@uninorte.edu.co, cjlascarro@uninorte.edu.co

Received: December 7th, de 2017. Received in revised form: October 10th, 2018. Accepted: November 2nd, 2018

Abstract
Experimental observations indicate that the mechanical behavior of clays is not only dependent on the stress and void ratio, but on its inherent anisotropy. The latter is the one arising from the material sedimentation process. In this work, the inherent anisotropy of a Kaolin clay is studied. For this purpose, soil samples are prepared with a proposed method producing samples with horizontal and vertical sedimentation axes. The samples go thru permeability tests, unconfined compression tests, oedometric compression tests and direct shear tests and the results carefully analyzed from the constitutive modeling point of view using the hypoplastic model for clays by [1]. Later, identify parameters depending on the inherent anisotropy; then perform some simulations to evaluate the model performance upon different samples with vertical and horizontal sedimentation angles. At the end, some concluding remarks are given.

Keywords: inherent anisotropy; clays; sample preparation method; hypoplastic model for clays.

Simulación de una arcilla Caolín con ejes de sedimentación vertical y horizontal

Resumen
Las observaciones experimentales indican que el comportamiento mecánico de las arcillas no solo depende de los esfuerzos y relaciones de vacíos, sino también de la anisotropía inherente. Esta última corresponde a la obtenida durante el proceso de sedimentación del material. En este trabajo, se estudia la anisotropía inherente de una arcilla Caolín. Para este propósito, se prepararon muestras de suelo con un método que permite producir muestras con ejes de sedimentación vertical y horizontal. Las muestras son posteriormente ensayadas en tests de permeabilidad, compresión inconfinada, oedométrico y corte directo. Los resultados son analizados cuidadosamente desde la perspectiva de la modelación constitutiva con el uso del modelo hipoplástico para arcillas de [1]. Los parámetros que dependen de la anisotropía inherente fueron identificados, y se evaluó el desempeño del modelo mediante simulaciones de distintas muestras con ejes de sedimentación horizontal y vertical. Finalmente, se presentan algunas conclusiones.

Palabras clave: anisotropía inherente; arcillas, método de preparación de muestras; modelo hipoplástico para arcillas.

1. Introduction

In soil mechanics, anisotropic materials are those whose mechanical properties are direction-dependent. This property is of relevant importance considering that most soils exhibit anisotropic behavior, especially when dealing with clay-like soils. Authors investigating this behavior agree with the distinction of two types of anisotropy: the inherent and induced anisotropy. This work focus only on the inherent anisotropy, which is the one emerging from the material deposition history, or in the case of laboratory samples, the one created during the sample preparation.

Several authors have examined the influence of the inherent anisotropy on permeability [2-5], strength and stiffness characteristics [6-11], stiffness for small strains [12], only to mention a few. Among many geotechnical applications, the effects of the soil anisotropy have been studied on slope stability e.g. [13-14], bearing capacity of

How to cite: Fuentes-Lacouture, W.M., Duque-Felfle, J.A. and Lascarro-Estrada, C.J., Constitutive simulation of a Kaolin clay with vertical and horizontal sedimentation axes. DYNA, 85(207), pp. 227-235, Octubre - Diciembre, 2018.

foundations e.g. [15-16], soil compressibility e.g. [17], deep excavations e.g. [18-20], and tunnels e.g. [21-22]. The aforementioned authors showed that the influence of the soil anisotropy is significant, and suggest their consideration on the prediction of geotechnical structures. Robust constitutive models able to simulate the mechanical behavior of clays are usually employed and evaluated to investigate the influence of the soil anisotropy on geotechnical applications. However, users of these models should be aware of those parameters that actually depend on the soil inherent anisotropy. There is very few literature devoted to investigate this dependence, and therefore more investigation in this direction is necessary.

In the present work, the inherent anisotropy of a Kaolin clay is studied. A special sample preparation method allows control of their sedimentation angle. Many samples with horizontal and vertical sedimentation axes are produced and subsequently tested. The experimental results are carefully analyzed aided by constitutive simulations of its mechanical response. For this purpose, it is employed the hypoplastic model for clays by [1]. Parameters of the constitutive model depending on the soil anisotropy are detected and calibrated considering their sedimentation axes. Finally, simulations of the performed experiments are submitted to evaluation and some limitations and other relevant observations are concluded. The notation of the article is as follows: scalar quantities are denoted with italic fonts (e.g. a, b), vectors with bold italic fonts (e.g. $\boldsymbol{a}, \boldsymbol{b}$), second rank tensor with bold fonts (e.g. $\mathbf{A}$, $\boldsymbol{\sigma}$), and fourth rank tensors with special fonts (e.g. $\boldsymbol{E}, \boldsymbol{L}$). Tensors represented with the indicial notation are denoted with italic symbols with their respective lower indices (e.g. A_{ij}, σ_{ij}). Multiplication with two dummy indices, also known as double contraction, is denoted with colon ":" (e.g. $\mathbf{A}\colon\mathbf{B} = A_{ij}B_{ij}$). When the symbol is omitted, it is understood a dyadic product (e.g. $\mathbf{AB} = A_{ij}B_{kl}$).

2. Experimental procedure

This section describes the experimental procedure conducted during this work and their results are given. The testing soil corresponds to a homogeneous Kaolin clay (silicate mineral). Characterization tests conducted on the Kaolin clay provided the following results. It presents a specific gravity of $G_s = 2.66$, a fine content (percent passing sieve #200) of 95%, a liquid limit of LL=27%, a plastic limit of PL=17% and plasticity index of PI=10%. According to the Unified Soil Classification System USCS, the Kaolin clay is a low plasticity clay. Table 1 summarizes the results. The clay mineral corresponds to a Kaolin produced by hydrolysis of potassium feldspar. Table 2 shows its chemical composition.

Table 1.
Characterization results for the Kaolin clay.

Parameter	Value
G_s	2.66
Fine content (%)	95
LL (%)	27
PL (%)	17
PI (%)	10
USCS classification	CL

Source: The Authors.

Table 2.
Chemical composition of the Kaolin clay.

Component	Percent (%)
SiO_2	48.0
Fe_2O_3	0.6
Al_2O_3	24.0
CaO	15.0
MgO	1.0
SO_3	0.1
Na_2O	1.2
K_2O	0.2
Igneous loss	9.9

Source: The Authors.

The sample preparation method begins with the production of a slurry resulting from the hydration of a dried Kaolin powder. A large quantity of water allows reaching 1.5 times its liquid limit, resulting in a mixture of about 1 kg of dried Kaolin for each 420 ml of water. The slurry is sufficiently soft to be manipulated on a large recipient Fig. 1 illustrates the sample preparation method. The slurry is then remolded and mixed by hand, until it reaches a homogenous state. In order to check for the homogeneity, several samples of slurry were tested in different positions to perform water content tests. All results evidenced that the water content of the slurry was almost homogeneous with a liquid limit of approximately 1.5 times the liquid limit (= 42 %). The mean water content was of 42% and the deviation standard was of 3.5%.

For the consolidation process, a special cylindrical mold to place the sample is used with dimensions of about 10 cm of diameter and 10 cm of height. Some filter papers cover the inner walls of the mold to assure an inner homogenous drainage of the sample during its initial consolidation process. After this, a certain amount of slurry is placed within the cylindrical mold, see Fig. 2. During the consolidation stage, a vertical load is applied on the top boundary of the sample while it drains through the bottom boundary. In order to guarantee a uniform bottom drainage, a box with compacted dry sand is placed underneath the sample, see Fig. 3a. The sand box has dimensions of 2.2 m long times 1.2 m width. The sand layer is properly compacted and horizontally levelled to produce a flat and rigid draining surface at the bottom of the sample. A high compaction effort helped to avoid significant settlement of the sand during the sample loading.

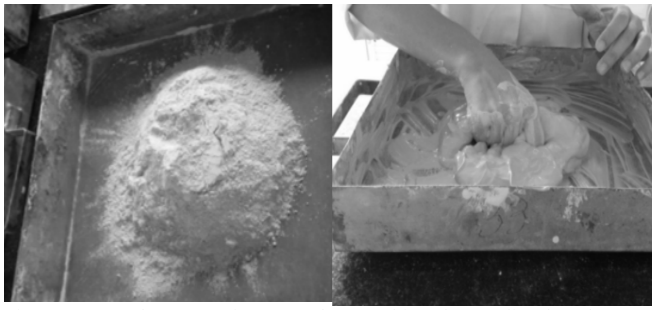

Figure 1. Sample preparation procedure: making the Kaolin clay slurry at 1.5 times the liquid limit. Left) Dried Kaolin powder. Right) Kaolin clay slurry after its hydration.
Source: The Authors.

The vertical load for the consolidation process is applied by assembling a piston to the top of the mold, see Fig. 3 (bottom). The piston induces a vertical stress depending on the selected weight. In order to avoid a tilted settlement of the sample, an increasing loading sequence was necessary with the following order: 10 kPa (8 kg) during the first day, 20 kPa (16 kg) during the second day and 40 kPa (32 kg) during the three subsequent days. Notice that the consolidation process takes about 5 days to produce good quality samples. The results with the selected loading sequence proved to produce homogenous samples with similar void ratios. After this procedure, samples were unloaded and carefully unconfined, see Fig. 4. At this point, all samples presented a vertical sedimentation axis coinciding with the gravity direction.

After their initial consolidation, samples received their final geometry with a special trimming device for clays shown in Fig. 5. Considering that the final sample diameter depends on the test to perform (e.g. unconfined compression, direct shear test, etc), different top plates compatible with the trimming device were produced with a 3D printer. The top plate of the trimming device (see Fig. 5 left)) was designed with the software SolidWorks and printed with a hard polymer. Two kind of samples were trimmed: samples with vertical sedimentation axes, hereafter identified with its sedimentation angle $\alpha = 0°$, and samples with horizontal sedimentation axes, i.e. $\alpha = 90°$. There is a schematic illustration of the trimming procedure to obtain the two different sedimentation axes in Fig. 6. With their final geometry, samples of Kaolin clay are proved to quantify the influence of the sedimentation angle on different properties, such as permeability and strain-stress characteristics. Next section describes the conducted experimental procedures and their results.

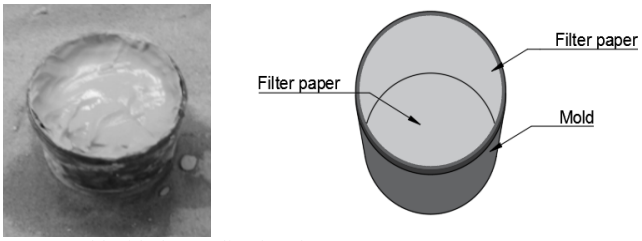

Figure 2. Mold with the Kaolin clay slurry.
Source: The Authors.

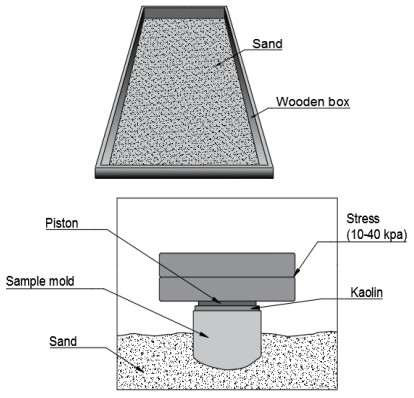

Figure 3. Top) Box with compacted dry sand as bottom drainage. Bottom) Mold subjected to a vertical load and placed on the sand box.
Source: The Authors.

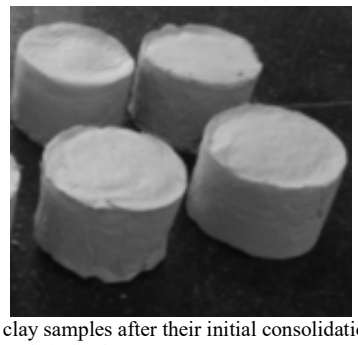

Figure 4. Kaolin clay samples after their initial consolidation process and before trimming to their final geometry.
Source: The Authors.

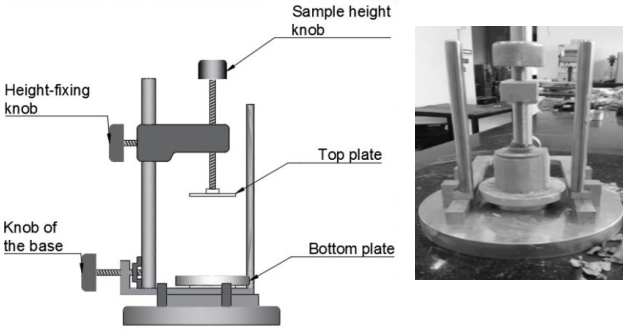

Figure 5. Clay trimming device to obtain the final sample geometry.
Source: The Authors.

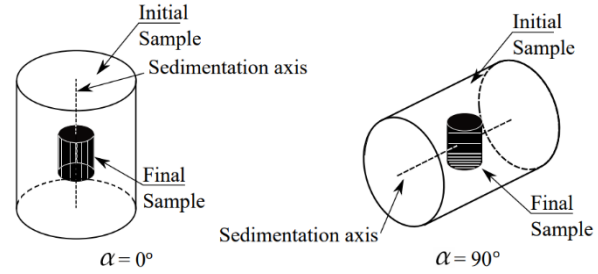

Figure 6. Schematic representation of the procedure to obtain the final sample geometry. Left) sample with vertical sedimentation axis. Right) with horizontal sedimentation axis.
Source: The Authors.

3. Experimental results

This section presents the experimental results of the Kaolin clay. Four different experiments on samples with horizontal $\alpha = 90°$ and vertical $\alpha = 0°$ sedimentation axes, named permeability tests, unconfined compression tests, oedometric tests and direct shear tests were executed. The following lines give and examine the results of each test.

The first corresponds to the permeability test. They were variable head permeability tests considering the low permeability of the Kaolin clay. Samples within the permeameter with a height of 3 cm were flooded with distilled water during two days to guarantee its complete saturation. After this procedure, samples with horizontal $\alpha = 90°$ and vertical $\alpha = 0°$ sedimentation axes were tested.

Table 3 shows the results of the permeability. All results showed that samples having a horizontal sedimentation axis $\alpha = 90°$ present a higher permeability than the ones with vertical sedimentation axes $\alpha = 0°$. The average permeability ratio $K(\alpha = 90°)/K(\alpha = 0°)$ is equal to 2.03. Similar results are in [2-4].

Table 3.
Results of permeability tests with Kaolin clay.

No.	e [-]	α[°]	K[cm/s]	Average
1	0,98		6,18E-7	
2	0,99	0	5,63E-7	5.94E-7
3	0,97	(vertical)	6,00E-7	
4	0.97		1,26E-6	
5	0.97	90	1,17E-6	1.21E-6
6	0.99	(horizontal)	1,21E-6	
			Ratio	2.03

Source: The Authors.

The next experiments correspond to unconfined compression tests. A total number of 10 samples are sheared, five of them having vertical sedimentation axis $\alpha = 0°$ and the others with horizontal sedimentation axis $\alpha = 90°$. The number of samples for each sedimentation angle allows us to evaluate the experiment reproducibility. The sample diameter was set to 6 cm and its height to 6 cm. The environmental humidity was under control to conserve samples under saturated conditions before shearing. Considering that all samples were prepared under the same conditions, they all had the same initial void ratio. All samples are sheared until reaching a vertical strain of about 25%. Fig. 7 shows the results of the unconfined compression tests show that they are qualitatively well reproducible. The experimental curves indicate that samples with horizontal sedimentation axis are softer than the others, i.e. the Young's modulus (for loading) E of samples with horizontal sedimentation angle $\alpha = 90°$ are lower than those with vertical sedimentation angle $\alpha = 0°$. The resulting ratio of the Young's modulus E between samples with horizontal and vertical sedimentation axes, $E(\alpha = 90°)$ and $E(\alpha = 0°)$ respectively, ranges between $E(\alpha = 90°)/\,E(\alpha = 0°) = \{0.6 \text{ to } 0.8\}$. Similarly, the ratio of unconfined shear strengths between samples with horizontal and vertical sedimentation axes ranges between $S_u(\alpha = 90°)/S_u(\alpha = 0°) = \{0.6 \text{ to } 0.8\}$. Table 4 summarizes the results of the unconfined compression tests.

Table 4.
Results of unconfined compression tests.

Parameter		Value
S_u [kPa] ($\alpha = 0°$)	Minimum	35
	Maximum	38
	Mean	36.5
S_u [kPa] ($\alpha = 90°$)	Minimum	26
	Maximum	28
	Mean	27
E [kPa] ($\alpha = 0°$)	Minimum	3800
	Maximum	4400
	Mean	4100
E [kPa] ($\alpha = 90°$)	Minimum	2300
	Maximum	2900
	Mean	2600

Source: The Authors.

The following experiments correspond to the oedometric compression tests, which included an unloading-reloading cycle. Two samples, one with horizontal and other with vertical sedimentation axis were tested. Special care produced very similar initial void ratios for both samples. Before proceeding with the oedometric compression, samples were flooded with distilled water within the oedometric apparatus during two days to guarantee their complete saturation. Fig. 8 shows the results and exhibit a similar pattern as by unconfined compression tests: samples with the horizontal sedimentation axis behave softer than the one of others. However, both experimental curves seem to yield to the same normal consolidation line for large stresses (mean stress $p > 100$ kPa). This behavior resembles some destructuration theories for clays [23], although their fundaments are associated with particle cementation and not with inherent anisotropy. On the other hand, unloading-reloading cycles showed a similar slope on both samples. The last observation suggests that elastic properties of the Kaolin clay are independent of its inherent anisotropy.

Finally, four different direct shear tests were performed, each of them having three points at normal stresses of approximately 50, 100 and 150 kPa. In total, 4 tests were conducted, two of them with samples having horizontal sedimentation axis $\alpha = 90°$ and the others with vertical sedimentation axis $\alpha = 0°$. It must be reminded that samples

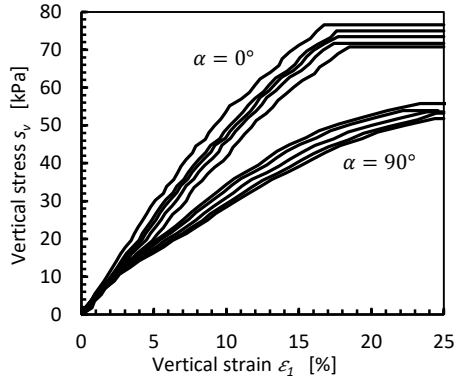

Figure 7. Unconfined compression test results of Kaolin clay.
Source: The Authors.

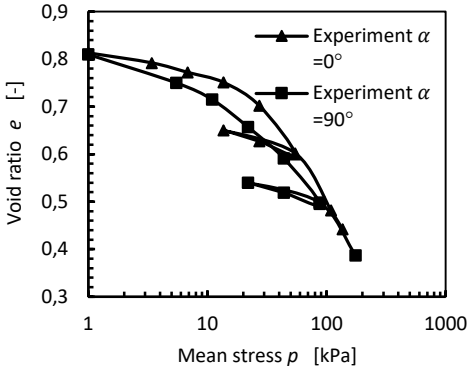

Figure 8. Results of the oedometric test.
Source: The Authors.

are expected to present very similar initial void ratios before placing them into the direct shear device. All samples received saturated distilled water during two days and subsequently consolidated to their respective normal stresses. After reaching the initial consolidation pressure, samples received shearing under a constant velocity of 0.05 mm/min to assure drained conditions.

The experimental results are in Fig. 9. Two main conclusions calls the attention: the first is the fact that all samples reached the same failure line. The fact that the failure condition was reached after large deformations without presenting a peak stress, indicates that the friction angle coincides with the critical state friction angle φ_c which resulted in approximately $\varphi_c = 20.5°$. The second is the difference between the initial stiffness for samples with vertical and horizontal sedimentation axes. Once more, samples with horizontal sedimentation axes are softer than those with vertical sedimentation axes, observation corroborated by the previous experimental results.

4. Brief description of the constitutive model and calibration

This section presents simulations of the experimental behavior of the Kaolin clay. This work applies the hypoplastic model for clays by [1]. The model is self-categorized as hypoplastic considering the fact that it lacks of a yield surface and resembles other former hypoplastic models for sands [24-25]. The hypoplastic model for clays is able to simulate the mechanical behavior of saturated clays under monotonic loading. Extensions for cyclic loading are also available in the literature [25-28], two of them proposed by the first author of this work, however, these extensions are not herein required.

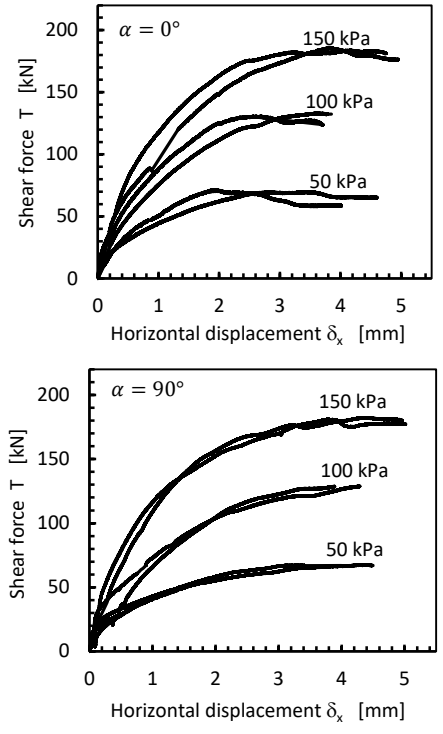

Figure 9. Direct shear test results. Top) Samples with vertical sedimentation angle $\alpha = 0°$. Bottom) Samples with horizontal sedimentation angle $\alpha = 90°$. Source: The Authors.

The general equation of the hypoplastic model for clays is:

$$\dot{\boldsymbol{\sigma}} = f_s \boldsymbol{\mathcal{L}} : \dot{\boldsymbol{\epsilon}} + f_s f_d \boldsymbol{N} \|\dot{\boldsymbol{\epsilon}}\| \quad (1)$$

Where $\dot{\boldsymbol{\sigma}}$ is the stress rate, $\dot{\boldsymbol{\epsilon}}$ is the strain rate, f_s, f_d are scalar factors, $\boldsymbol{N}$ is the non-linear stiffness (second order tensor) and $\boldsymbol{\mathcal{L}}$ is the linear stiffness (fourth order tensor). Deduction and analysis of the constitutive is in [1] and [29], but is out of the scope of the present article. The model requires the calibration of five material parameters: $\varphi_c, \lambda^*, \kappa^*, N$ and r. A brief description of their calibration procedure is given in Appendix 8.2 and their names, approximate range and some useful experiments for their calibration are listed in Table 5. The constitutive model has been implemented in a Fortran subroutine UMAT compatible with the commercial software Abaqus Standard. Implemented is an explicit integration scheme with substepping algorithm in which a very small substepping size has been selected to assure numerical convergence. The material subroutine is previously tested in many simulations and showed agreement with other reported simulations, e.g. [1] and [29].

Two sets of material parameters passed calibration for samples with horizontal and vertical sedimentation axes respectively. Upon the calibration procedure, it has been detected, that while parameters λ^*, N depend on the soil sedimentation axis, κ^*, φ_c and r seem to be constant and independent on the material inherent anisotropy. The fact that the critical state friction angle φ_c remains constant, is in agreement with some other authors e.g. [30].The calibrated parameters are listed in Table 6. Notice that the ratio of λ^* (=0.77) is within the range obtained for the Young modulus from unconfined compression tests (=0.6-0.8), see section 3.

Table 5.
Parameters of the hypoplastic model for clays.

	Name	Approx. Range	Useful experiment
N	Constant for normal consolidation line	0.1-10	Oedometric test
λ^*	Butterfield loading index	0.01-1	Oedometric test
κ^*	Butterfield swelling index	0.001-0.1	Oedometric test
r	Stiffness factor	0-3	Triaxial test, direct shear test
φ_c	Critical state friction angle	5°-45°	Triaxial test, direct shear test

Source: The Authors.

Table 6.
Values of the material parameters for horizontal and vertical sedimentation angle.

	$\alpha = 90°$	$\alpha = 0°$	Ratio ($\alpha = 90°/\alpha = 0°$)
N	0.79	0.92	0.86
λ^*	0.085	0.11	0.77
κ^*	0.011	0.011	1
r	0.3	0.3	1
φ_c	20.5	20.5	1

Source: The Authors.

5. Simulations of experimental results

In this section, oedometric and direct shear tests with the Kaolin clay are simulated. The hypoplastic model for clays by [1] is employed using the parameters from Table 6. The following lines analyze the simulation performance.

The first test corresponds to the oedometric compression, and is given in Fig. 10. The simulation assumed element test conditions, i.e. the stress and strain fields were assumed to be homogenous. The simulations showed agreement with the oedometric curves. The unloading-reloading cycle was also simulated although the model lacks of small stiffness effects.

The simulations of direct shear tests are now analyzed. These simulations cannot assume element test conditions (homogenous field) considering the induced shear band produced to the sample. Therefore, its simulation has been performed with a finite element Boundary Value Problem (BVP). The sample has a circular shape with a diameter of 6.35 cm and height of 2 cm. No geometry partition has been made to avoid the use of interface elements between the top and bottom bodies of the sample. The mesh is shown Fig. 11(top). The test was simulated under drained conditions, and hence 3D finite element for static analysis are employed. No gravity has been considered due to the small height of the sample. The initial conditions for vertical stresses and void ratio were given in accordance with the experimental measurements, which are reported in Table 7. An example of

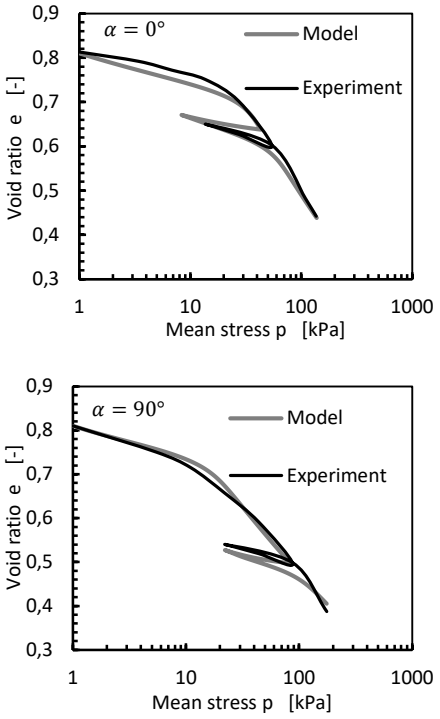

Figure 10.Simulation of oedometric tests with Kaolin clay. Top) samples with vertical sedimentation axis $\alpha = 0°$. Bottom) samples with horizontal sedimentation axis $\alpha = 90°$.
Source: The Authors.

Table 7.
Initial conditions for the simulation of the direct shear test.

Vertical stress [kPa]	Initial void ratios	
	$\alpha = 0°$	$\alpha = 90°$
50	0.63	0.57
100	0.53	0.49
150	0.46	0.44

Source: The Authors.

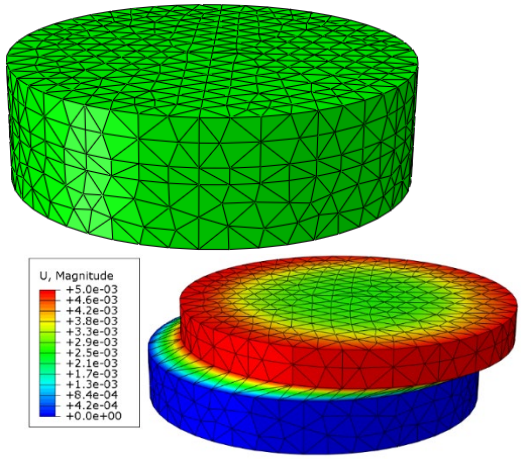

Figure 11. Finite element model for the direct shear test. Top) mesh of the model. Bottom) contours of displacements at the end of the simulation for $\alpha = 0$.
Source: The Authors.

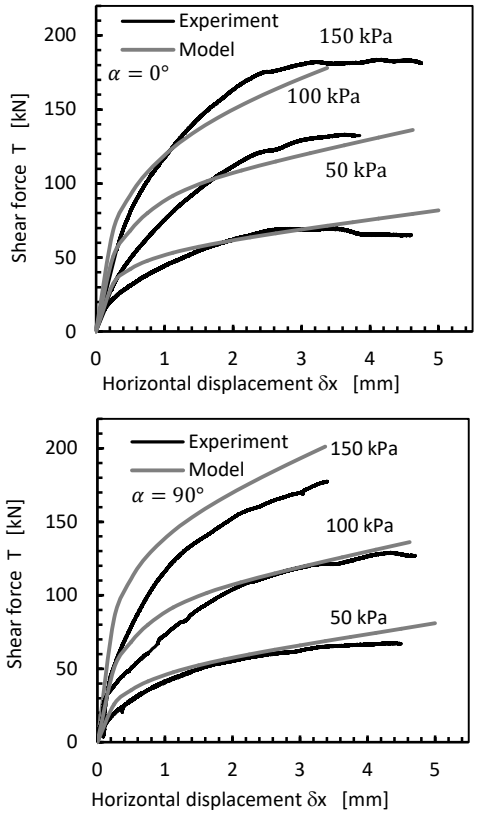

Figure 12. Simulations of direct shear test. Top) samples with vertical sedimentation axis $\alpha = 0°$. Bottom) samples with horizontal sedimentation axis $\alpha = 90°$.
Source: The Authors.

its distorted mesh after the simulation is shown in Fig. 11(bottom). The results in the space of shear force T against horizontal displacement δ_x are shown in Fig. 12 and exhibit accurate predictions of the model. Small discrepancies are observed for the case of the sample with horizontal sedimentation axis $\alpha = 90°$, Fig. 12(bottom).

6. Simulation of a bearing capacity problem

Finally, the influence of the inherent anisotropy is analyzed in a Boundary Value Problem (BVP). The problem simulates a rigid strip foundation with a width of 1 m supported by the ground surface. This analysis considers 2D finite elements under plane strain conditions. Fig 13 shows the dimension and mesh of the BVP. We assumed that the soil is dry, and therefore drained conditions under static analysis. For the sake of simplicity, the strip foundation load is simulated with the application of a vertical displacement of -0.7 m. The resulting reaction force below the foundation is analyzed to compute the ultimate bearing capacity. The BVP is repeated twice, one with parameters for vertical sedimentation axis $\alpha = 0°$ and the second for horizontal sedimentation axis $\alpha = 90°$.

The initial conditions are as follows. An initial vertical stress resulting from the gravity load with a constant (dry) specific weight of $\gamma_d = 15\ \text{kN/m}^3$ is considered. Initial horizontal stresses are computed with a lateral earth coefficient of $K_0 = 0.65$. The initial void ratio are computed following the Butterfield relation for normal consolidation line $\log((1+e)) = N - \lambda^* \log(p * F)$ with parameters for $\alpha = 0\,°$ and assuming a factor of F=1.5. The latter factor F has been computed as an approximation to reproduce the behavior of a normally consolidated clay under oedometric (and not isotropic) conditions. Horizontal displacements are restrained at the lateral boundaries while vertical displacements are restrained at the bottom boundary. Fig. 14 shows an example of the final contours of the deviator stress $q = \sqrt{(3/2)}\ ||\ \boldsymbol{\sigma}^*\ ||$.

Fig. 15 shows simulated results. The plot shows the resulting reaction vertical stress against the settlement. The result resembles the conclusions from the unconfined compression test and direct shear test, in which an initial softer behavior of the soil with horizontal sedimentation axis exists. There exists some discrepancies at the maximum reaction vertical force. This suggests that the ultimate bearing capacity of the soil depends on the inherent anisotropy.

7. Final remarks

The inherent anisotropy of a Kaolin clay has been tested and analyzed. The experimental results shows a significant influence of the inherent anisotropy. Permeability tests indicates a higher permeability for samples with horizontal sedimentation axis. The ratio is approximately of two times with respect to the vertical permeability. The influence of the inherent anisotropy is also confirmed on the stress-strain behavior reported by the unconfined compression test, oedometric test and direct shear test. They all showed that samples with horizontal sedimentation angles exhibit softer stiffness during shearing.

The calibration process using the hypoplastic model for clays demonstrated some parameters not affected by the material inherent anisotropy. This is the case of the swelling index κ^*, critical state friction angle φ_c and stiffness factor r. These parameters are responsible of the elastic response and critical state of the soil. Finally, a simulation of a bearing capacity problem using finite elements showed that consideration of the material anisotropy is of importance in some geotechnical problems and should not be ignored. Currently, there is more investigation to study the effect of the inherent anisotropy under cyclic conditions.

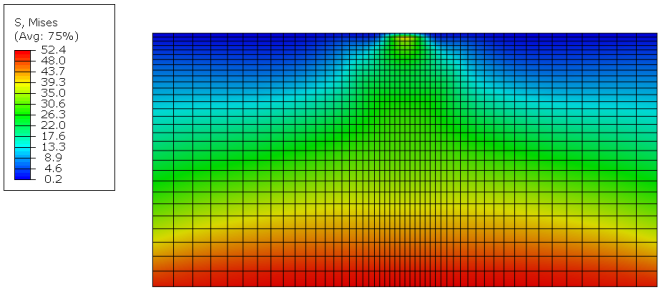

Figure 14. Contours of the deviator stress $q = \sqrt{\frac{3}{2}}\ ||\ \boldsymbol{\sigma}^*\ ||$. Values in kPa.
Source: The Authors.

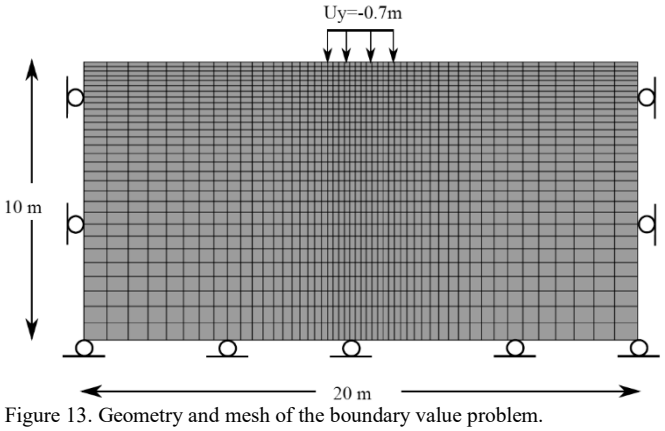

Figure 13. Geometry and mesh of the boundary value problem.
Source: The Authors.

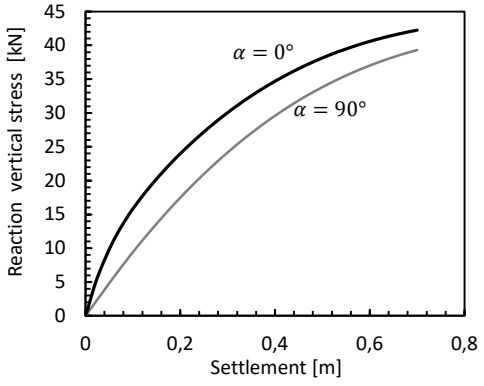

Figure 15. Reaction vertical stress under the footing.
Source: The Authors.

Appendix

Hypoplastic model for clays

The general relation of the hypoplastic model for clays is [1]:

$$\dot{\boldsymbol{\sigma}} = f_s \boldsymbol{\mathcal{L}} : \dot{\boldsymbol{\epsilon}} + f_s f_d \mathbf{N} \|\dot{\boldsymbol{\epsilon}}\| \tag{2}$$

Where $\dot{\boldsymbol{\sigma}}$ is the stress rate, $\dot{\boldsymbol{\epsilon}}$ is the strain rate, f_s, f_d are scalar factors, $\boldsymbol{N}$ is the non-linear stiffness (second-rank tensor) tensor defined as:

$$\mathbf{N} = \boldsymbol{\mathcal{L}} : (-Y \frac{\mathbf{m}}{\|\mathbf{m}\|}) \tag{3}$$

Where Y is the degree of non-linearity, $\boldsymbol{m}$ is the hypoplastic flow rule and $\boldsymbol{\mathcal{L}}$ is the hypoelastic stiffness (fourth rank tensor):

$$\boldsymbol{\mathcal{L}} = 3(c_1 \boldsymbol{I} + c_2 a^2 \hat{\boldsymbol{\sigma}} \otimes \hat{\boldsymbol{\sigma}}) \tag{4}$$

Where $\boldsymbol{I}$ is a second–order unity tensor, $I_{ijkl} = \frac{1}{2}(1_{ik}1_{jl} + 1_{il}1_{jk})$ is a fourth-order unity tensor and the stress dependent magnitudes are defined as:

$$\mathrm{tr}\boldsymbol{\sigma} = \boldsymbol{\sigma}\mathbf{:1}, \quad \hat{\boldsymbol{\sigma}} = \frac{\boldsymbol{\sigma}}{\mathrm{tr}\boldsymbol{\sigma}}, \quad \hat{\boldsymbol{\sigma}}^* = \hat{\boldsymbol{\sigma}} - \mathbf{1}/3 \tag{5}$$

The scalar factor a is defined as:

$$a = \frac{\sqrt{3}(3 - \sin\varphi_c)}{2\sqrt{2}\sin\varphi_c} \tag{6}$$

The degree of nonlinearity Y considers the Matsuoka-Nakai yield surface for failure conditions and is:

$$Y = (\mathrm{Y}_0 - 1)\frac{(I_1 I_2 + 9I_3)(1 - \sin^2\varphi_c)}{8I_3 \sin^2\varphi_c} + \mathrm{Y}_0 \tag{7}$$

With $Y_0 = \sqrt{3}a/(3 + a^2)$ and I_1, I_2 and I_3 being the stress invariants defined as:

$$I_1 = \mathrm{tr}\boldsymbol{\sigma}, \qquad I_2 = 0.5\,[\boldsymbol{\sigma}\mathbf{:}\boldsymbol{\sigma} - (I_1)^2], \quad I_3 = \det\boldsymbol{\sigma} \tag{8}$$

The hypoplastic flow rule $\boldsymbol{m}$ reads:

$$\mathrm{m} = -\frac{a}{F}\left[\hat{\boldsymbol{\sigma}} + \hat{\boldsymbol{\sigma}}^* - \frac{\hat{\boldsymbol{\sigma}}}{3}\left(\frac{6\hat{\boldsymbol{\sigma}}\mathbf{:}\hat{\boldsymbol{\sigma}} - 1}{\left(\frac{F}{a}\right)^2 + \hat{\boldsymbol{\sigma}}\mathbf{:}\hat{\boldsymbol{\sigma}}}\right)\right] \tag{9}$$

With factor F given by:

$$F = \sqrt{\frac{1}{8}\tan^2\psi + \frac{2 - \tan^2\psi}{2 + \sqrt{2}\tan\psi cos3\theta}} - \frac{1}{2\sqrt{2}}\tan\psi \tag{10}$$

Where the angles ψ and θ are computed from the relations:

$$\tan = \sqrt{3}\|\hat{\boldsymbol{\sigma}}^*\|, \qquad cos3\theta = -\sqrt{6}\frac{\mathrm{tr}(\hat{\boldsymbol{\sigma}}^* \cdot \hat{\boldsymbol{\sigma}}^* \cdot \hat{\boldsymbol{\sigma}}^*)}{[\hat{\boldsymbol{\sigma}}^* \cdot \hat{\boldsymbol{\sigma}}^*]^{3/2}} \tag{11}$$

Barotropy and pyknotropy factors f_s and $f_d$read

$$f_s = -\frac{\mathrm{tr}\boldsymbol{\sigma}}{\lambda^*}\left(3 + a^2 - 2^\alpha a\sqrt{3}\right)$$
$$f_d = \left[-\frac{2\mathrm{tr}\boldsymbol{\sigma}}{3p_r}\exp\left(\frac{\ln(1 + \mathrm{e}) - N}{\lambda^*}\right)\right]^\alpha \tag{12}$$

Where p_r is the reference stress 1 kPa and the scalar quantity is α is calculated by:

$$\alpha = \frac{1}{\ln 2}\ln\left[\frac{\lambda^* - \kappa^*}{\lambda^* + \kappa^*}\left(\frac{3 + a^2}{a\sqrt{3}}\right)\right] \tag{13}$$

Finally, factors c_1 and c_2 are as follows:

$$c_1 = \frac{2(3 + a^2 - 2^\alpha a\sqrt{3})}{9r}$$
$$c_2 = 1 + (1 - c_1)\frac{3}{a^2} \tag{14}$$

Short guide for material parameters calibration

The hypoplastic model for clays requires the calibration of 5 parameters: $\varphi_c, \lambda^*, \kappa^*, N$ and r. A simple calibration procedure is in the following lines. Analysis and details of these parameters may be found elsewhere [30]:

- Critical friction angle φ_c: it may be calibrated under triaxial test or direct shear test for points lying at large deviator strains $\varepsilon_s > 20\%$.
- Butterfield compression index λ^*: can be adjusted to the points lying on the normal consolidation line according to the Butterfiled relation $\log((1 + e_1)/(1 + e_2)) = -\lambda^* \log(p_2/p_1)$.
- Butterfiled swelling index κ^*: can be adjusted to the points lying under a unloading-reloading cycle on an oedometric test following the relation $\log((1 + e_1)/(1 + e_2)) = -\kappa^* \log(p_2/p_1)$.
- Constant for normal consolidation line N: can be adjusted from the points lying on the normal consolidation line under isotropic conditions according to the Butterfield relation $\log((1 + e)) = N - \lambda^* \log(p)$.
- Shear stiffness factor r: can be adjusted by trial and error to match the shear stiffness under triaxial or direct shear test shearing.

Acknowledgement

The authors appreciate the financial support given by COLCIENCIAS for the project with code 1215748-59323 from the convocation 748-2016.

Bibliography

[1] Mašín, D., A hypoplastic constitutive model for clays. International Journal for Numerical and Analytical Methods in Geomechanics, 29(4), pp. 311-336, 2005. DOI: 10.1002/nag.416
[2] Al-Tabbaa, A. and Wood, D., Some measurements of the permeability of kaolin. Géotechnique, 38(3), pp. 453-454, 1988. DOI: 10.1680/geot.1988.38.3.453
[3] Olsen, H., Nichols, R. and Rice, T., Low gradient permeability measurements in a triaxial system. Géotechnique, 35(2), pp. 145-157, 1985. DOI: 10.1680/geot.1985.35.2.145
[4] Pane, V., Croce, P., Znidarcic, H. and Ko, H., Effects of consolidation on permeability measurements for soft clays. Géotechnique, 33(1), pp. 67-72, 1983. DOI: 10.1680/geot.1983.33.1.67
[5] Basak, P., Soil structure and its Effects on Hydraulic Conductivity. Soil Science, 114(6), pp. 417-422, 1972. DOI: 10.1097/00010694-197212000-00003
[6] Brosse, A., Study of the anisotropy of three british mudrocks using a hollow cylinder apparatus. PhD dissertation, Department of Civil Engineering, Imperial College London, 2012.
[7] Jardine, R. and Zdravkovic, H., Some anisotropic stiffness characteristics of a silt under general stress conditions. Géotechnique, 47(3), pp. 407-437, 1997. DOI: 10.1680/geot.1997.47.3.407
[8] Chua, K., Dunstan, T. and Arthur, J., Induced anisotropy in a sand. Géotechnique, 27(1), pp. 13-30, 1977. DOI: 10.1680/geot.1977.27.1.13
[9] Oda, M., Initial fabrics and their relations to the mechanical properties of granular materials. Soils and Foundations, 12(1), pp. 17-36, 1972. DOI: 10.3208/sandf1960.12.17
[10] Hight, D., Bond, A. and Legge, J., Characterization of the Bothkennar Clay - an overview. Géotechnique, 42(2), pp. 303-347, 1992. DOI: 10.1680/geot.1992.42.2.303
[11] Kuwano, R. and Jardine, R., On the applicability of cross-anisotropic elasticity to granular materials at very small strains. Géotechnique, 52(10), pp. 727-749, 2002. DOI: 10.1680/geot.2002.52.10.727
[12] Mašín, D. and Rott, J., Small strain stiffness anisotropy of natural sedimentary clays: review and a model. Acta Geotechnica, 9(2), pp. 299-312, 2014. DOI: 10.1007/s11440-013-0271-2
[13] Lo, K., Stability of slopes in anisotropic soil. Journal of the Soil Mechanics and Foundations Division, 91(4), pp. 85-106, 1965.
[14] Al-Karni, A. and Al-Shamrani, M., Study of the effect of soil anisotropy on slope stability using method of slices. Computers and Geotechnics, 26(2), pp. 83-103, 2000. DOI: 10.1016/S0266-352X(99)00046-4
[15] Meyerhof, G., Bearing capacity of anisotropic cohesionless soils. Canadian Geotechnical Journal, 15(4), pp. 592-595, 1978. DOI: 10.1139/t78-063
[16] Siddiquee, M., Tanaka, T., Tatsuoka, F., Tani, K. and Morimoto, T., Numerical simulation of bearing capacity characteristics of strip footing on sand. Soils and Foundations, 39(4), pp. 93-109, 1999. DOI: 10.3208/sandf.39.4_93
[17] Smith, P., The behaviour of natural high compressibility clay with special reference to construction on soft ground. PhD dissertation, Department of Civil Engineering, Imperial College London, 1992.
[18] Burland, J., Longworth, T. and Moore, J., Study of ground movement and progressive failure caused by a deep excavation in Oxford Clay. Géotechnique, 27(4), pp. 557-591, 1977. DOI: 10.1680/geot.1977.27.4.557
[19] Pierpoint, N., The prediction and back analysis of excavation behaviour in Oxford Clay. PhD dissertation, Department of Civil Engineering, University of Sheffield, 1996.
[20] Pennington, D., The anisotropic small strain stiffness of Cambridge Gault Clay. PhD dissertation, Department of Civil Engineering, University of Bristol, 1999.
[21] Lee, K. and Rowe, R., Deformations caused by surface loading and tunnelling; the role of elastic anisotropy. Géotechnique, 39(1), pp. 125-140, 1989. DOI: 10.1680/geot.1989.39.1.125
[22] Hosseini, R., Experimental study of the geotechnical properties of UK mudrocks. PhD dissertation, Department of Civil Engineering, Imperial College London, 2012.
[23] Baudet, B. and Stallebrass, S., A constitutive model for structured clays. Géotechnique, 54(4), pp. 269-278, 2004. DOI: 10.1680/geot.2004.54.4.269
[24] Wolffersdorff, P., A hypoplastic relation for granular materials with a predefined limit state surface. Mechanics of Cohesive-Frictional Materials, 1(3), pp. 251-271, 1996. DOI: 10.1002/(SICI)1099-1484(199607)1:3<251::AID-CFM13>3.0.CO;2-3
[25] Niemunis, A., Extended hypoplastic models for soils. Dissertation for habilitation, Bochum, Germany, 2002.
[26] Niemunis, A. and Herle, I., Hypoplastic model for cohesionless soils with elastic strain range. Mechanic of cohesive-frictional materials, 2(4), pp. 279-299, 1997.
[27] Poblete, M., Fuentes, W. and Triantafyllidis, T., On the simulation of multidimensional cyclic loading with intergranular strain. Acta Geotechnica, 11(6), pp. 1263-1285, 2016. DOI: 10.1007/s11440-016-0492-2
[28] Fuentes, W., Triantafyllidis, T. and Lascarro, C., Evaluating the performance of an ISA-Hypoplasticity constitutive model on problems with repetitive loading. In: Holistic Simulation of Geotechnical Installation Processes, Lecture Notes in Applied and Computational Mechanics, pp. 341-362, Springer, 2017. DOI: 10.1007/978-3-319-52590-7_16
[29] Mašín, D., Hypoplastic models for fine-grained soils. PhD dissertation, Charles University, Prague, 2006.
[30] Fuentes, W. and Triantafyllidis, T., ISA: A constitutive model for deposited sand. in Aktuelle Forschung in der Bodenmechanik, Bochum, pp. 169-187, Springer, 2015. DOI: 10.1007/978-3-662-45991-1_10

Fuentes W., received the BSc. in Eng in Civil Engineering in 2007, the BSc. Eng in Environmental Engineering in 2008, the MSc. degree in Civil Engineering with Emphasis in Geotechnical Engineering in 2009, all of them from the University Los Andes, Colombia, and the PhD degree in Engineering in 2014 in Karlsruhe Institute of Technology KIT, Germany. Currently, he is professor in University del Norte. His research interests include geotechnical simulation, soil anisotropy and constitutive models for soils.
ORCID: 0000-0002-9281-3871

Duque, J., received the BSc. Eng in Civil Engineering in 2016 and the MSc. degree in Civil Engineering in 2018 all of them form the University del Norte, Colombia. His research interests include geotechnical simulation, soil anisotropy, constitutive models for soils and pavements.
ORCID: 0000-0002-9663-1741

Lascarro, C., received the BSc. Eng in Civil Engineering in 2012 in University de Cartagena, Colombia. Currently, he is student for the PhD. degree in Civil Engineering in University del Norte, Colombia. His research interests include geotechnical simulation, soil anisotropy and constitutive models for soils.
ORCID: 0000-0002-7041-0107.